Front. Mater. Sci. 2019, 13(3): 305–313
https://doi.org/10.1007/s11706-019-0472-1

RESEARCH ARTICLE

Wearable gas/strain sensors based on reduced graphene oxide/linen fabrics

Xia HE (✉)[1], Qingchun LIU[2], Jiajun WANG[1], and Huiling CHEN[1]

1 School of Art and Design, Zhejiang Sci-Tech University, Hangzhou 310018, China
2 School of Art Design, Zhejiang A&F University, Hangzhou 311300, China

ABSTRACT: Multifunctional wearable e-textiles have been a focus of much attention due to their great potential for healthcare, sportswear, fitness, space, and military applications. Among them, electroconductive textile yarn shows great promise for use as the next-generation flexible sensors without compromising properties and comfort of usual textiles. Recently, a myriad of efforts have been devoted to improving performance and functionality of wearable sensors. However, the current manufacturing process of metal-based electroconductive textile yarn is expensive, unscalable, and environmentally unfriendly. In this work, we report the preparation of multifunctional reduced graphene oxide/linen (RGO/LN) fabrics through the reduction and the followed suction filtration. As-prepared RGO/LN fabric could serve as the methane gas sensor, which exhibited high sensitivity, remarkable reliability and feasibility. Furthermore, the RGO/LN fabric sensor exhibited good moisture permeability and air permeability. The present work reveals that RGO/LN fabric has great potential as wearable smart devices in personal healthcare applications.

KEYWORDS: wearable sensor; reduced graphene oxide; linen fabric; methane

Contents

Received June 13, 2019; accepted July 17, 2019

E-mail: hexia2000@163.com

1 Introduction

Wearable electronics have drawn widespread consideration and also have gained respectable progress in recent years [1–5]. As a pivotal sub-portion of wearable electronics, flexible strain sensors with features of conformal adhesion to arbitrary and soft surfaces exhibit substantive potential applications in electronic skins [6–7], human-machine

interaction [8–9], emotion detection [10–11], sound recognition [12–13], personalized health monitoring [14–15], and others.

There are mainly two components of flexible strain sensors based on the piezoresistive effect, i.e., elastic polymer matrices, which enable flexibility and durability of the whole device, and conductive sensing elements, which predominate electromechanical properties of strain sensors [16–17]. Flexible strain sensors with desirable performance should satisfy the demands of superb sensitivity, extraordinary stretchability, stability, durability, and fast response as well as other demands [18]. However, current technologies for wearable garments are associated with a number of challenges that other electronic technologies do not face, such as the complex and time-consuming manufacturing process of e-textiles and the use of expensive, nonbiodegradable, and unstable metallic conductive materials. Apart from standard requirements for electronics and sensing capabilities, there are requirements for such e-textiles to be breathable, washable, flexible, wearable, and produced using an environmentally friendly manufacturing process [19–20].

With the rapid development of nanotechnology, researchers began to utilize nanomaterials, such as metallic nanowires, metallic thin films and carbon nanomaterials, as functional sensing elements for the design of flexible strain sensors, which show promising features for the fabrication of highly sensitive and stretchable strain sensors. Graphene has attracted a great deal of interest because of its extremely high charge-carrier mobilities, extraordinary thermodynamic stability, excellent mechanical stiffness, exceptional electron emission properties, applicability in photonic propulsion and green chemistry processes, and suitability for both interconnects and active devices (transistors and sensors) [21–23]. Furthermore, it was reported that graphene has superior thermal conductivity than those of metals and carbon nanotubes and demonstrates the potential to circumvent self-heating problems of electronic devices at elevated temperature [24–25]. Reduced graphene oxide (RGO), a form of graphene, can be produced in scalable quantities in a stable dispersion [26–27]. Recently various investigations have focused the application of RGO for wearable e-textiles because of its ability to interact with oxygen-containing groups in textile fibers, which would therefore become part of the textiles rather than forming only a surface coating [28–30]. For instance, Wang's group fabricated a freestanding, flexible, foldable and large-area ultrathin RGO paper with high thermal conductivity and sensitive electrothermal response, which can be applied to prepare bifunctional personal thermal management devices for heating and cooling [31]. Zhou et al. prepared N-doping of RGO film on polydimethylsiloxane (PDMS), which displays excellent tensile properties for stress sensors [32]. Yin and coworkers fabricated novel strain sensors based on reduced graphene oxide woven fabrics (GWFs) by pyrolyzing commercial cotton bandages coated RGO [33]. The GWF strain sensor was successfully used to monitor full-range (both subtle and vigorous) human activities or physical vibrational signals of the local environment.

On the other hand, cellulose is one of the most available and renewable biopolymers. Cellulose active sites, i.e. OH groups, especially in amorphous areas of the cellulose structure, can be chemically modified via etherification, esterification, graft copolymerization and/or crosslinking to produce cellulose derivatives with desirable properties. Potential applications of cellulose-based textile materials in daily life as well as medical-use textiles, after modification and functionalization, have recently gained more consideration reflecting their favorable properties namely availability, biodegradability, hydrophilicity, comfortability, eco-friendly in addition to chemical reactivity. Linen (LN) is classified as the cellulose-based textile with numerous hydroxyl groups, and has a great recognition in the fashion industry as well as among consumers for its casual look, elegance and grace. Its special attributes like comfort, freshness and hygiene made its way to apparels and non-apparels and brought LN into the curiosity domain of researchers. However, to the best of our knowledge, until now there has no report on LN fabrics in the field of wearable electronics.

In present work, LN fabrics were selected as the substrate, on which RGO was coated to prepare flexible LN fabric sensor. The prepared RGO/LN fabric can serve as methane gas and strain sensor, which exhibited high sensitivity, remarkable reliability and feasibility.

2 Experimental

2.1 Materials

Graphite powder (GP) was purchased from Sinopharm Chemical Reagent Co., Ltd., China. LN fabrics (226 g/m^2) were kindly provided by the Textile Processing Laboratory of Zhejiang University of Technology, China. Other reagents included $KMnO_4$, H_2O_2 (Sanying Chemical

Reagent Co., Ltd., Shanghai, China), $NaBH_4$, and NH_4OH (Gaojingxi Chemical Co., Ltd., Hangzhou, China). All reagents were used as received without further purification.

2.2 Methods

2.2.1 Synthesis of GO

The GO dispersion was prepared on the basis of natural GP according to a modified Hummers' method [34]. Briefly, GP (1 g) was dispersed in H_2SO_4 (120 mL) and $NaNO_3$ (1 g), followed by the slow addition of $KMnO_4$ (6 g) under ice bath condition and agitation. Then, the reaction was maintained at room temperature for 48 h to completely oxidize of graphite. Subsequently, the mixture was diluted by distilled water and certain H_2O_2 until the color of the mixture changed from brown to bright yellow. Finally, the product was washed several times with 10% HCl and distilled water to give the yellow GO dispersion.

2.2.2 Preparation of RGO

GO (30 mg) was dissolved in 50 mL deionized (DI) water and stirred for 30 min, and excess $NaBH_4$ was put into the solution to reduce GO. The mixture was stirred for 2 h to decompose the remaining $NaBH_4$, and then the pH of the solution was tuned to neutral by adding 0.1 mol/L HNO_3. The black dispersion was washed several times to remove any residuals and finally diluted into DI water to adjust the concentration of the RGO dispersion at ~2 mg/mL.

2.2.3 Preparation of RGO/LN fabrics

RGO aqueous dispersions were obtained through ultrasonication for 2 h, and there were different concentrations of final RGO dispersions, 50 mg/100 mL, 100 mg/100 mL and 150 mg/100 mL, denoted as RGO-50, RGO-100 and RGO-150, respectively, as shown in Fig. 1. Then, 100 mL as-prepared RGO dispersions were forced to be coated on LN fabrics by the suction filtration process (funnel radius: 120 mm). Finally, the finished samples were dried at a lower drying temperature (100 °C) and cured at 150 °C for 3 min to produce RGO/LN fabrics.

2.3 Characterization

Morphologies of the samples were determined by field emission scanning electron microscopy (FESEM, ZEISS VLTRA-55, Germany) at 3 kV and transmission electron microscopy (TEM) using a JEOL instrument (JEM-2010 HR, Japan) operating at 200 kV. Energy dispersive X-ray analysis (EDX, IncaEnergy-200) was used to investigate sample compositions. Crystal structures of GO and RGO powders were evaluated with X-ray diffraction (XRD, ARL-XTRA Thermo ARL Co., Ltd., Switzerland) and Raman spectrometer (LabRAM HR Evolution, French HORIBA). Water vapor transmission (WVT) rates of RGO/LN fabrics were measured by gravimetric analysis with a WVP tester (TSY-T3, Labthink, China). The conductivity was measured with a electrometer (34460A, Agilent, USA). All samples were tested five times in the same condition and the average values were used.

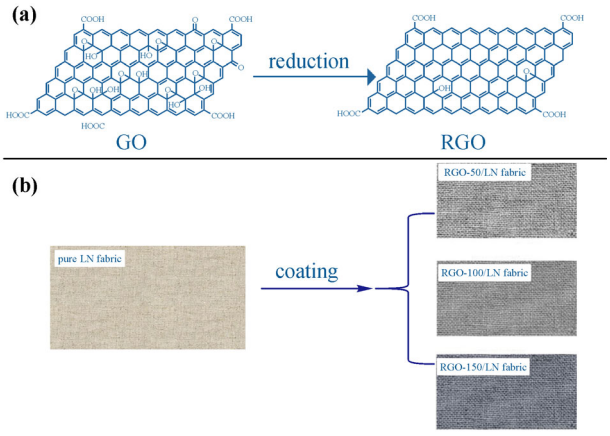

Fig. 1 **(a)** Molecular structures of GO and RGO. **(b)** Digital photos of RGO/LN fabric samples.

2.4 Measurement of fabric performances

The waterproofness of the fabric was evaluated by measuring the hydrostatic pressure at a hydrostatic pressure test equipment (YG812C, Ningbo Textile Instruments Co., Ltd., China) according to the AATCC 127 standard with a pressurization rate of 6.0 kPa·min^{-1}. The WVT rate representing the breathable performance was measured according to the ASTM E96 inverse cup standards by using a WVT test equipment (YG 601H, Ningbo Textile Instruments Co., Ltd., China) under the constant temperature of 38 °C and the relative humidity of 50%. The WVT rate (η, unit: g·m^{-2}·d^{-1}) was calculated as follow:

$$\eta = \frac{m_1 - m_2}{S} \times 24 \quad (1)$$

where m_1 is the mass of the test cup before the test, m_2 is the mass of the test cup after the test, and S is the test area. The air permeability of the fabric was measured under a

differential pressure of 100 Pa according to the ASTM D 737 criterion. Results of the hydrostatic pressure, the WVT rate and the air permeability were obtained from three measurements per sample. Mechanical properties were measured on a universal material testing machine (Instron 3365, America).

3 Results and discussion

3.1 Preparation and characterization of GO and RGO

The preparation process of RGO/LN fabrics is depicted schematically in Fig. 2. GO sheets were reduced by $NaBH_4$, and subsequently the black dispersion was deposited on the surface of LN fabrics through the suction filtration. After drying and curing at 150 °C, the color of the fabric changed to metallic black and the RGO/LN fabric still exhibited instinctive flexibility like textile materials.

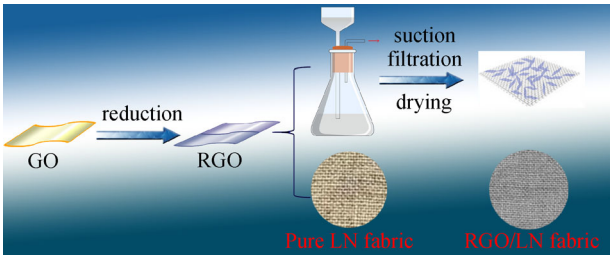

Fig. 2 The preparation process of RGO/LN fabrics.

The morphologies of as-prepared GO and RGO were observed by TEM. Figure 3 shows TEM images of GO sheets obtained by the Hummers method (Fig. 3(a)) and as-prepared RGO (Fig. 3(b)) reduced by $NaBH_4$. Lamellar structures of GO and RGO with compacted layers can be clearly seen. High resolution transmission electron microscopy (HRTEM) was employed to investigate the selected area framed in the thin sheet. As for RGO, more corrugation and scrolling simultaneously viewed are inevitable owing to that the colloid stability was destroyed when oxygen groups in GO were removed. As shown in Fig. 5(b), the edge of the RGO sheet is rather thinner than that of GO, indicating that RGO has fewer compacted layers in comparison with those of GO, which may result in better electric performance [35].

The compositions of GO and RGO were evaluated by EDX. As shown in Fig. 4, the oxygen content of GO was 12.6%, while that of RGO was only 3.4%, proving that most of oxygen-containing functional groups of GO had been reduced.

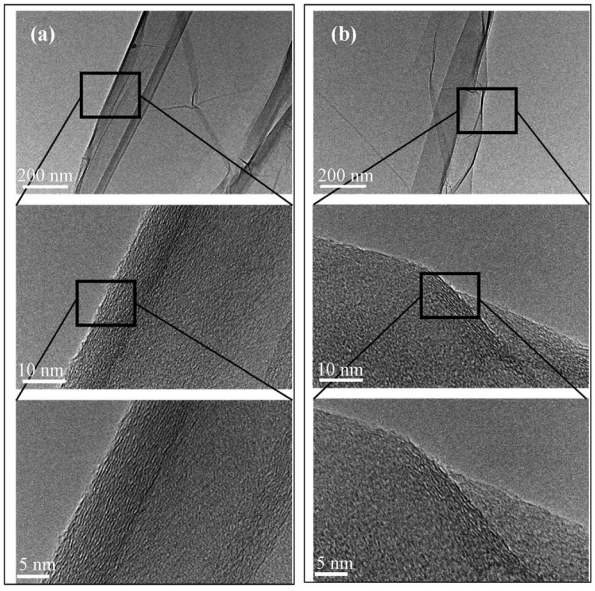

Fig. 3 TEM images of **(a)** GO and **(b)** RGO.

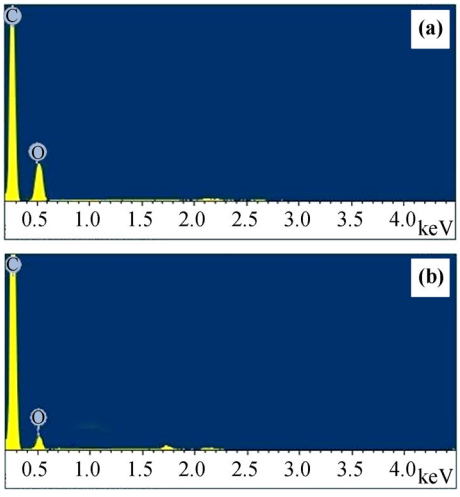

Fig. 4 EDX spectra of **(a)** GO and **(b)** RGO.

3.2 Preparation and characterization of RGO/LN fabrics

After coating of RGO sheets on LN fabrics, the surface morphologies of different samples were observed through SEM. As shown in Figs. 5(a) and 5(b), the pristine LN fabric had a relatively smooth surface with little impurities and grooves due to the natural growth of the LN fabric. Figures 5(c) and 5(d) show GO sheets coated on the LN fabric (GO/LN fabric) used as a reference sample exhibiting flake-like structures and wrinkled edges. Figures 5(e) and 5(f) show RGO/LN fabric, which did not change a lot in comparison with GO/LN fabric, and the fibers were still wrapped by RGO sheets completely. It can be seen that after coating of GO and RGO by the suction filtration, GO

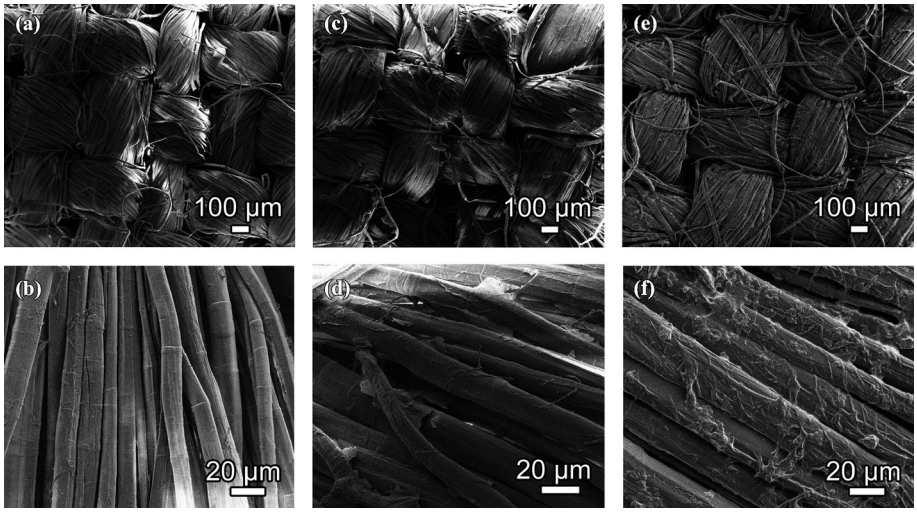

Fig. 5 SEM images of **(a)(b)** pure LN fabric, **(c)(d)** GO/LN fabric (GO-100), and **(e)(f)** RGO/LN fabric (RGO-100).

and RGO sheets were attached to the surface of LN fibers compactly and continuously, suggesting successful wrapping of GO and RGO onto the surface of LN fabrics.

The structural analysis of our proposed system RGO-100/LN with GO-100/LN fabric as the reference sample was made via XRD and Raman spectroscopy (Fig. 6(a)). XRD was used to study crystalline phases of the samples, and the interplanar spacing (*d*-spacing) between GO and RGO layers can be determined by the Bragg's equation [36]. It is well known that graphite has a higher diffraction peak at 26.7°, which represents that the layer spacing of GP is 3.34 Å. After the chemical oxidation, the peak shifted to 10.27°, indicating that the *d*-spacing of GO coated on the LN fabric be increased to 8.60 Å. The XRD patterns show broad diffraction (0 0 2) peaks at around 24.16° for RGO/LN fabric, corresponding to the interlayer spacing at about 3.68 Å, quite close to 3.34 Å of the original graphite phase. The fact also indicates that RGO coated on the LN fabric was almost completely reduced [37].

After coating of GO and RGO sheets, the Raman spectrum showed two typical peaks at 1350 and 1606 cm^{-1} attributed to the D peak and the G peak [38–39], respectively, as presented in Fig. 6(b). The intensity ratio of the D peak to the G peak (I_D/I_G) is usually considered for characterizing the relative defect structure [40–41]. The I_D/I_G ratio of RGO/LN fabric was 1.02, while that of GO/LN fabric was 0.88, indicating that the chemical reduction converted the structure of GO sheets with plenty of structural defects, consistent with the characterization of TEM results.

Mechanical strength values were also measured for RGO/LN fabric (RGO-100) and GO/LN fabric (GO-100) compared with that of pure LN fabric, as shown in Fig. 6(c). Values of the tensile strength and the breaking elongation were 43.4 MPa and 5.9% for RGO/LN fabric, 29.5 MPa and 6.4% for GO/LN fabric, and 18.4 MPa and 7.7% for pure LN fabric, respectively. Uniaxial tensile tests indicated that the enhancement of strength was prominent after the deposition of RGO sheets. The RGO-100/LN fabric sample showed the best mechanical strength among all three (data are not shown here).

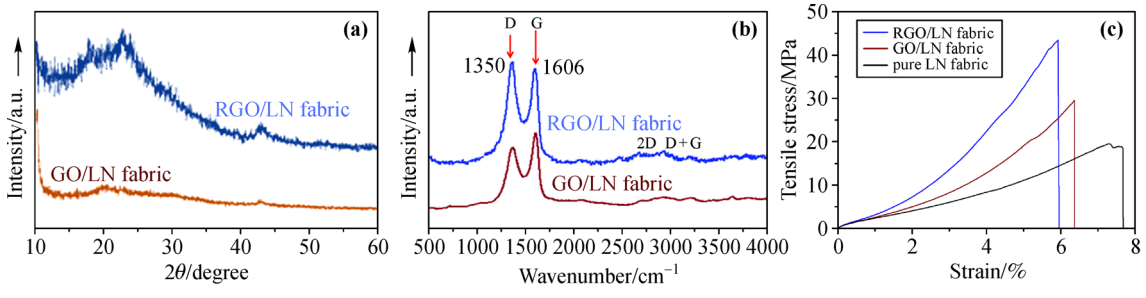

Fig. 6 **(a)** Raman spectra of GO/LN fabric (GO-100) and RGO/LN fabric (RGO-100). **(b)** XRD patterns of GO/LN fabric (GO-100) and RGO/LN fabric (RGO-100). **(c)** Typical stress–strain curves of LN fabric, GO/LN fabric (GO-100) and RGO/LN fabric (RGO-100).

3.3 WVT and air permeability of RGO/LN fabrics

The moisture transportation through fabrics is one of the key factors for fabric comfort. For wearer comfort, the moisture management has the function of transporting sweat away from the skin and evaporating it to the atmosphere and also that of the weight control of cloth by preventing moisture increase on the fabric. Moisture transport properties of textiles are obtained from perspiration in liquid and vapor forms, which influences the dynamic comfort in practical use.

The breathable performance was evaluated by measuring WVT rates of fabric samples. It is well known that the entry-level breathable WVT grade for fabrics should be in the range of 1500–5000 $g \cdot m^{-2} \cdot d^{-1}$, and the LN fabric has a higher WVT rate than that of the cotton fabric. Figure 7(a) implies a comparison of moisture permeability data between pure LN fabric and LN fabric with different amounts of the RGO coating. As shown in Fig. 7(a), although the coating amount of RGO increased, η decreased gradually: η values of RGO-50/LN fabric, RGO-100/LN fabric and RGO-150/LN fabric were 3856, 3463 and 3066 $g \cdot m^{-2} \cdot d^{-1}$, respectively. This may be attributed to that with the increase of the coating amount of RGO, the accumulation of nanosheets blocks the interspace of the fabric, leading to the decrease of the fabric porosity. However, η values of all samples were still in the range of 3066–4322 $g \cdot m^{-2} \cdot d^{-1}$, well meeting the entry-level breathable WVT grade. The air permeability shown in Fig. 7(b) also indicated similar tendency as that of WVT.

3.4 Gas sensing measurements of RGO/LN fabrics

Figures 8(a)–8(c) show responses of sensors based on

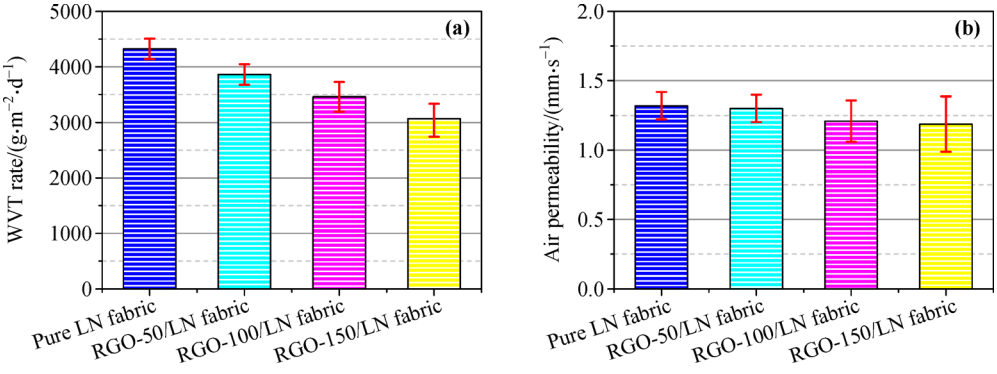

Fig. 7 **(a)** The WVT rates and **(b)** the air permeability of LN fabric and RGO/LN fabric samples.

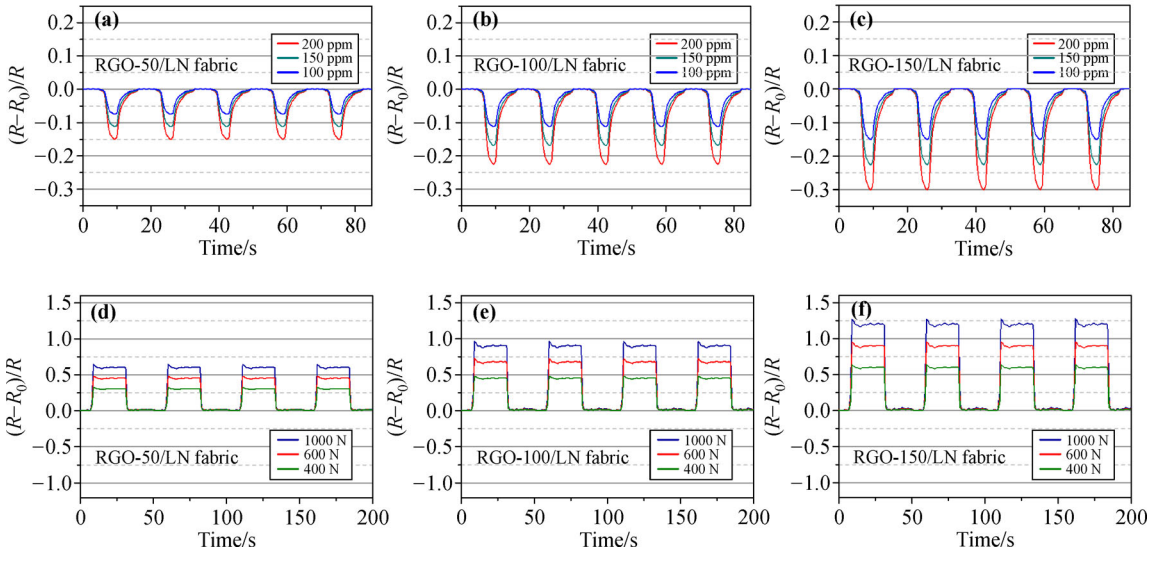

Fig. 8 Sensitivities of RGO/LN fabric-based sensors to the CH_4 gas at different concentrations: **(a)** RGO-50/LN fabric; **(b)** RGO-100/LN fabric; **(c)** RGO-150/LN fabric. Normalized resistance changes of RGO/LN fabrics under different strains: **(d)** RGO-50/LN fabric; **(e)** RGO-100/LN fabric; **(f)** RGO-150/LN fabric.

RGO/LN fabrics to different concentrations of the CH_4 gas at room temperature. During the exposure of the device to different concentrations of the CH_4 gas, the obvious resistance change can be achieved for the case of the gas concentration from 100 to 200 ppm (1 ppm = 10^{-6}), indicating that the response of the device clearly depends on the CH_4 gas concentration. It is clear that even at the ppm level, the RGO/LN-based sensing device exhibited fast response and recovery performance. With the increase of the CH_4 gas concentration, the resistance of the device increased accordingly. This result reveals that RGO nanostructure-based gas sensors be candidates in promising application for the actual CH_4 gas detection under the atmosphere condition.

The high sensitivity of RGO/LN fabric is attributed to the small size of RGO nanosheets, which provides a large number of surface reactive sites for CH_4 molecules [42–43]. At first, oxygen molecules were adsorbed onto the surface of the LN fabric and ionized into oxygen anions, forming a hole accumulation layer [44]. When the CH_4 gas was introduced, CH_4 molecules decomposed to produce CH_3 and H radicals on the surface of RGO/LN fabric, and H radical reacted with O^-, which could be detected by the RGO/flax fabric sensor described as follows [45–46]:

$$O_2 + 2e^- \rightarrow 2O^- \quad (2)$$

$$CH_4 \rightarrow CH_3 + H \quad (3)$$

$$4H^+ + 4O^- \rightarrow 2[H_2O_2] \rightarrow 2H_2O + O_2 \quad (4)$$

Figures 8(d)–8(f) show normalized sensor response curves of RGO/LN fabric samples under different strains. All of RGO/LN fabrics exhibited good strain-response behaviors. During the pressure loading, RGO/LN fabrics were compressed immediately, namely, the RGO layer was pressed into stacking layers, resulting in the conductive channel of the sensor. It can be seen that with the increase of the coating amount of RGO, the normalized sensor response increased. For an individual sensor, with the increase of the strain, the normalized sensor response increased. This property can be used for flexible pressure sensors.

Figure 9 illustrates the influence of the loading amount of RGO on the sensor gauge factor. It can be observed that the increase of the loading amount of RGO can increase the gauge factor. Figure 10 suggests the remarkable reliability and the durability of RGO/LN fabrics. The resistance

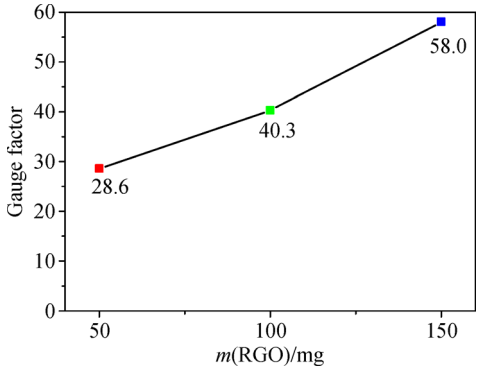

Fig. 9 The Gauge factor of composites under different conditions.

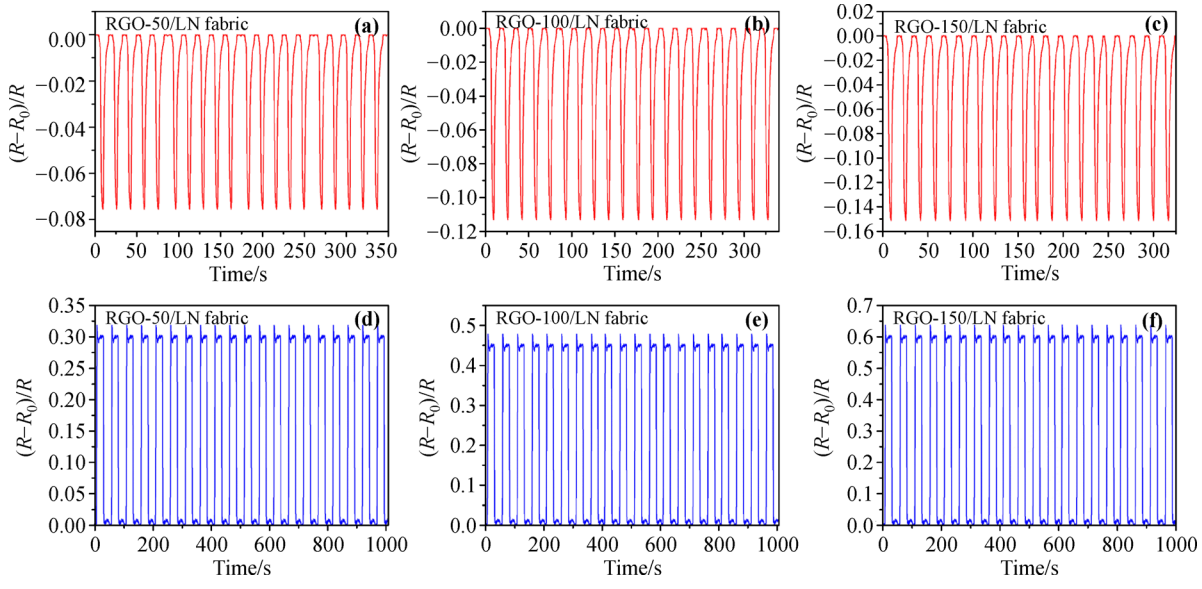

Fig. 10 The application of RGO-LN fabrics for the CH_4 sensor under 350 cycles: **(a)** RGO-50/LN fabric; **(b)** RGO-100/LN fabric; **(c)** RGO-150/LN fabric. The application of RGO-LN fabrics for the strain sensor under 1000 cycles: **(d)** RGO-50/LN fabric; **(e)** RGO-100/LN fabric; **(f)** RGO-150/LN fabric.

against the mechanical damage of the composite fabric was further evaluated by a laundering test using the RGO-100/LN fabric sample. As shown in Fig. 11, even the response of the sensor slightly decreased with the increase of laundering cycles, the obvious resistance change can be achieved when the device was exposed to 200 ppm CH_4 gas.

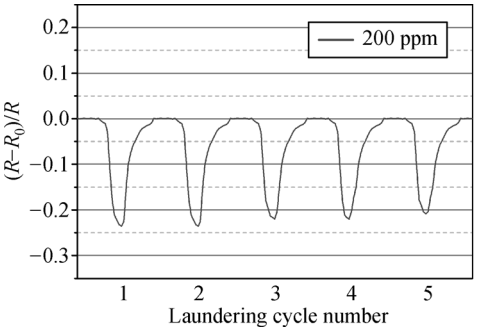

Fig. 11 The sensitivity of the RGO-100/LN fabric-based sensor to 200 ppm CH_4 gas with laundering cycles.

4 Conclusions

In this paper, multifunctional RGO/LN fabrics were prepared via the reduction and the followed suction filtration. As-prepared RGO/LN fabrics served as the methane gas and strain sensors, which exhibited high sensitivity, remarkable reliability and feasibility. Furthermore, the RGO/LN fabric sensor exhibited good washability, moisture permeability and gas permeability, revealing its great potential in the application of wearable flexible sensors in various critical environments.

Disclosure of potential conflicts of interests The authors declare that they have no conflicts of interest.

References

[1] Cheng T, Zhang Y, Lai W Y, et al. Stretchable thin-film electrodes for flexible electronics with high deformability and stretchability. Advanced Materials, 2015, 27(22): 3349–3376

[2] Wang X, Dong L, Zhang H, et al. Recent progress in electronic skin. Advanced Science, 2015, 2(10): 1500169

[3] Amjadi M, Kyung K U, Park I, et al. Stretchable, skin-mountable, and wearable strain sensors and their potential applications: A review. Advanced Functional Materials, 2016, 26(11): 1678–1698

[4] Zhao S, Li J, Cao D, et al. Recent advancements in flexible and stretchable electrodes for electromechanical sensors: strategies, materials, and features. ACS Applied Materials & Interfaces, 2017, 9(14): 12147–12164

[5] Jang H, Park Y J, Chen X, et al. Graphene-based flexible and stretchable electronics. Advanced Materials, 2016, 28(22): 4184–4202

[6] Guo Q, Huang B, Lu C, et al. A cephalopod-inspired mechano-luminescence material with skin-like self-healing and sensing properties. Materials Horizons, 2019, 6(5): 996–1004

[7] Jeong Y R, Park H, Jin S W, et al. Highly stretchable and sensitive strain sensors using fragmentized graphene foam. Advanced Functional Materials, 2015, 25(27): 4228–4236

[8] Liu X, Tang C, Du X, et al. A highly sensitive graphene woven fabric strain sensor for wearable wireless musical instruments. Materials Horizons, 2017, 4(3): 477–486

[9] Amjadi M, Pichitpajongkit A, Lee S, et al. Highly stretchable and sensitive strain sensor based on silver nanowire-elastomer nanocomposite. ACS Nano, 2014, 8(5): 5154–5163

[10] Liu X, Su G, Guo Q, et al. Hierarchically structured self-healing sensors with tunable positive/negative piezoresistivity. Advanced Functional Materials, 2018, 28(15): 1706658

[11] Zhang X, Cao J, Yang Y, et al. Flame-retardant, highly sensitive strain sensors enabled by renewable phytic acid-doped biotemplate synthesis and spirally structure design. Chemical Engineering Journal, 2019, 374: 730–737

[12] Cheng Y, Wang R, Sun J, et al. A stretchable and highly sensitive graphene-based fiber for sensing tensile strain, bending, and torsion. Advanced Materials, 2015, 27(45): 7365–7371

[13] Park B, Kim J, Kang D, et al. Dramatically enhanced mechano-sensitivity and signal-to-noise ratio of nanoscale crack-based sensors: effect of crack depth. Advanced Materials, 2016, 28(37): 8130–8137

[14] Wang Y, Wang L, Yang T, et al. Wearable and highly sensitive graphene strain sensors for human motion monitoring. Advanced Functional Materials, 2014, 24(29): 4666–4670

[15] Zhang M, Wang C, Wang H, et al. Carbonized cotton fabric for high-performance wearable strain sensors. Advanced Functional Materials, 2017, 27(2): 1604795

[16] Shi G, Zhao Z, Pai J H, et al. Highly sensitive, wearable, durable strain sensors and stretchable conductors using graphene/silicon rubber composites. Advanced Functional Materials, 2016, 26(42): 7614–7625

[17] Wang C, Li X, Gao E, et al. Carbonized silk fabric for ultrastretchable, highly sensitive, and wearable strain sensors. Advanced Materials, 2016, 28(31): 6640–6648

[18] Liu Z, Qi D, Guo P, et al. Thickness-gradient films for high gauge factor stretchable strain sensors. Advanced Materials, 2015, 27(40): 6230–6237

[19] Zeng W, Shu L, Li Q, et al. Fiber-based wearable electronics: a

review of materials, fabrication, devices, and applications. Advanced Materials, 2014, 26(31): 5310–5336

[20] Afroj S, Karim N, Wang Z, et al. Engineering graphene flakes for wearable textile sensors via highly scalable and ultrafast yarn dyeing technique. ACS Nano, 2019, 13(4): 3847–3857

[21] Novoselov K S, Geim A K, Morozov S V, et al. Electric field effect in atomically thin carbon films. Science, 2004, 306(5696): 666–669

[22] Geim A K. Graphene: status and prospects. Science, 2009, 324 (5934): 1530–1534

[23] He Q, Wu S, Yin Z, et al. Graphene-based electronic sensors. Chemical Science, 2012, 3(6): 1764–1772

[24] Balandin A A, Ghosh S, Bao W, et al. Superior thermal conductivity of single-layer graphene. Nano Letters, 2008, 8(3): 902–907

[25] Sun P, Zhu M, Wang K, et al. Small temperature coefficient of resistivity of graphene/graphene oxide hybrid membranes. ACS Applied Materials & Interfaces, 2013, 5(19): 9563–9571

[26] Karim N, Afroj S, Tan S, et al. Scalable production of graphene-based wearable e-textiles. ACS Nano, 2017, 11(12): 12266–12275

[27] Ren J, Wang C, Zhang X, et al. Environmentally-friendly conductive cotton fabric as flexible strain sensor based on hot press reduced graphene oxide. Carbon, 2017, 111: 622–630

[28] Abdelkader A M, Karim N, Vallés C, et al. Ultraflexible and robust graphene supercapacitors printed on textiles for wearable electronics applications. 2D Materials, 2017, 4(3): 035016

[29] Zhao S, Guo L, Li J, et al. Binary synergistic sensitivity strengthening of bioinspired hierarchical architectures based on fragmentized reduced graphene oxide sponge and silver nanoparticles for strain sensors and beyond. Small, 2017, 13(28): 1700944

[30] Yun Y J, Hong W G, Kim W J, et al. A novel method for applying reduced graphene oxide directly to electronic textiles from yarns to fabrics. Advanced Materials, 2013, 25(40): 5701–5705

[31] Guo Y, Dun C, Xu J, et al. Ultrathin, washable, and large-area graphene papers for personal thermal management. Small, 2017, 13(44): 1702645

[32] Zhou H P, Ye X, Huang W, et al. Wearable, flexible, disposable plasma-reduced graphene oxide stress sensors for monitoring activities in austere environments. ACS Applied Materials & Interfaces, 2019, 11(16): 15122–15132

[33] Yin B, Wen Y, Hong T, et al. Highly stretchable, ultrasensitive, and wearable strain sensors based on facilely prepared reduced graphene oxide woven fabrics in an ethanol flame. ACS Applied Materials & Interfaces, 2017, 9(37): 32054–32064

[34] Hummers W S, Offeman R E. Preparation of graphitic oxide. Journal of the American Chemical Society, 1958, 80(6): 1339

[35] Chen Y, Zhang X, Zhang D, et al. High performance supercapacitors based on reduced graphene oxide in aqueous and ionic liquid electrolytes. Carbon, 2011, 49(2): 573–580

[36] Eslamian M. Spray-on thin film PV solar cells: advances, potentials and challenges. Coatings, 2014, 4(1): 60–84

[37] Yasin G, Arif M, Shakeel M, et al. Exploring the nickel–graphene nanocomposite coatings for superior corrosion resistance: manipulating the effect of deposition current density on its morphology, mechanical properties, and erosion-corrosion performance. Advanced Engineering Materials, 2018, 20(7): 1701166

[38] Ferrari A C, Robertson J. Interpretation of Raman spectra of disordered and amorphous carbon. Physical Review B, 2000, 61 (20): 14095–14107

[39] Tuinstra F, Koenig J L. Raman spectrum of graphite. The Journal of Chemical Physics, 1970, 53(3): 1126–1130

[40] Dresselhaus M S, Jorio A, Souza Filho A G, et al. Defect characterization in graphene and carbon nanotubes using Raman spectroscopy. Philosophical Transactions: Mathematical, Physical and Engineering Sciences, 2010, 368(1932): 5355–5377

[41] Shen J, Hu Y, Shi M, et al. Fast and facile preparation of graphene oxide and reduced graphene oxide nanoplatelets. Chemistry of Materials, 2009, 21(15): 3514–3520

[42] Miller D R, Akbar S A, Morris P A. Nanoscale metal oxide-based hetero-junctions for gas sensing: A review. Sensors and Actuators B: Chemical, 2014, 204: 250–272

[43] Vuong N M, Hieu N M, Kim D, et al. Ni_2O_3 decoration of In_2O_3 nanostructures for catalytically enhanced methane sensing. Applied Surface Science, 2014, 317: 765–770

[44] Kim H J, Lee J H. Highly sensitive and selective gas sensors using p-type oxide semiconductors: Overview. Sensors and Actuators B: Chemical, 2014, 192: 607–627

[45] Vuong N M, Hieu N M, Hieu H N, et al. Ni_2O_3-decorated SnO_2 particulate films for methane gas sensors. Sensors and Actuators B: Chemical, 2014, 192: 327–333

[46] Cho N G, Hwang I S, Kim H G, et al. Gas sensing properties of p-type hollow NiO hemispheres prepared by polymeric colloidal templating method. Sensors and Actuators B: Chemical, 2011, 155 (1): 366–371